Desalination and Water Treatment
www.deswater.com

doi: 10.5004/dwt.2017.20195

63 (2017) 227–240
February

Phosphate removal and recovery using lime-iron sludge: adsorption, desorption, fractal analysis, modeling and optimization using artificial neural network-genetic algorithm

Beverly S. Chittoo, Clint Sutherland*

Project Management and Civil Infrastructure Systems, The University of Trinidad and Tobago, San Fernando Campus, Trinidad (WI), Tel. 868 497 5744; email: clint.sutherland@utt.edu.tt (C. Sutherland); Tel. 868 491 6879; email: beverly.chittoo@utt.edu.tt (B.S. Chittoo)

Received 7 April 2016; Accepted 23 August 2016

ABSTRACT

An artificial neural network (ANN) was developed to predict the adsorption of phosphate by lime-iron sludge. A fitness function derived from the ANN was incorporated within a genetic algorithm (GA) to elucidate the most optimal combination of operational parameters. The adsorbent characteristics were examined through SEM imagery and analyzed by fractal analysis. Batch experiments were conducted and modeled to expound the mechanisms of adsorption. Kinetic data were best simulated using the diffusion-chemisorption model while equilibrium data followed the Langmuir isotherm. Film and intra-particle diffusion were the dominant transport mechanisms while physisorption was the dominant attachment mechanism. Lime-iron sludge exhibited a maximum adsorption capacity of 15.3 mg/g and compared well with other reported adsorbents. ANN-GA optimization revealed maximum adsorption at an initial phosphate concentration of 59 mg/L, sludge dose of 3 g and temperature of 325 K. The ANN-GA prediction was subsequently verified through laboratory experiments which revealed an excellent prediction.

Keywords: Adsorption; Fractal analysis; Lime-iron sludge; Phosphate; Thermodynamics; Artificial neural network; Genetic algorithm

1. Introduction

Phosphorus is a non-renewable resource, and global reserves are estimated to last up to 2035, after which demand will exceed supply [1]. Additionally, it is an essential nutrient for living organisms and a key component of many industrial processes [2]. As a consequence, phosphate is frequently introduced into water bodies from domestic and agro-industrial wastewater [3]. The presence of this limiting nutrient, above permissible discharge levels, can stimulate the extraordinary growth of algae, destroy aquatic life, disrupt the natural food chain and lead to deterioration of water quality [4]. Consequently, the recovery of phosphate from wastewater is worthwhile prior to its discharge into water bodies.

Physical-chemical processes such as ion exchange, dissolved air flotation, membrane filtration, high-rate sedimentation, and adsorption are used for phosphorus treatment [5]. Adsorption is one of the most common techniques used for phosphate removal due to its simplicity of design and operation, insensitivity to toxic pollutants and potential to produce a high quality treated effluent [6].

In the past, several studies have investigated the removal of phosphate using low-cost adsorbents such as blast furnace slags [7], iron oxide tailings [8], fly ash [9], red mud [10], and alum sludge [11]. These materials were reported to efficiently remove phosphate from wastewater. Major components in the materials for phosphate removal were identified to be aluminum hydroxide, iron oxide, calcium oxide, and calcium carbonate [11].

Adsorption processes may be influenced by several variables including temperature, agitation speed, initial adsorbate concentration, adsorbent dose, solution pH, conductivity, contact time and presence of other competitive species [12–14]. Optimization

* Corresponding author.

is therefore necessary to achieve maximum performance. This is frequently performed by varying one parameter at a time while keeping all others constant. The single variable optimization method provides valuable insight regarding the mechanisms of adsorption; however, it ignores the interaction effects of multiple parameters and may not provide an accurate representation of the process. In order to overcome this limitation, several studies have investigated the use of artificial neural network (ANN) to model adsorption processes [15–17]. This statistical design approach studies the input–output relationships of known data to predict unknown relationships. ANN has the ability to model highly non-linear phenomena. This makes it an efficient predictive tool to represent even the most complex systems while at the same time save cost and time required for experimental studies [18]. The drawback of ANN lies in the selection of input parameters prior to training. These parameters influence the success of training, but there are no definite set of rules for its selection [19]. Furthermore, ANN also suffers from difficulty in trapping into local minima and overfitting. These weaknesses are frequently eliminated by combining ANN with genetic algorithm (GA) [20].

GA is a stochastic global search algorithm which simulates the theory of evolution by natural selection while searching for a fitness function that helps in its natural optimization [21]. Several authors have used the GA methodology for the optimization of adsorption processes based on weights and biases obtained from ANN. It was associated with ANN to optimize the adsorption of methylene blue and brilliant green from aqueous solution by graphite oxide nanoparticle [22]. ANN-GA optimization was also successfully used to predict the removal of lead ions from aqueous solutions using intercalated tartrate-Mg–Al layered double hydroxides. The predicted and actual percentages of lead ions removal were 101.2% and 98.7%, respectively [21]. Similarly, high correlation was reported using a GA-ANN for methane adsorption onto activated carbon [23].

The objectives of this investigation are (1) to describe the process of phosphate adsorption onto lime-iron sludge through batch kinetic, equilibrium, and desorption studies; (2) to elucidate the mechanisms of adsorption aided by simulation using mathematical models; (3) to develop an ANN model to predict the phosphate adsorption capacity of lime-iron sludge; and (4) to optimize the amount of phosphate adsorbed using an ANN-GA approach.

2. Materials and methods

2.1. Chemicals and adsorbents

2.1.1. Preparation of adsorbent

The sludge used in this study was generated from iron removal processes at a water treatment plant located in central Trinidad. The influent groundwater at this plant contains an exceptionally high iron content of approximately 15.0 mg/L, due to the geology of the source aquifers [24]. In order to meet WHO acceptable standard of 0.3 mg/L, hydrated lime is added to increase the pH of the water and allow added chlorine to react with and precipitate the iron as sludge. This sludge has an iron content of approximately 60% which is significantly higher than values reported in the literature and is therefore defined in this study as lime-iron sludge. Alum and lime sludge was obtained from a water treatment plant located in north and central Trinidad respectively. After collection, the samples were heated in an oven (ELE78-1215/01) at 378 K for 24 h and then cooled to room temperature for 72 h. It was then pulverized using a mortar and pestle and sieved to pass a 2.36 mm sieve.

2.1.2. Preparation of adsorbate

Phosphate stock solution was prepared by dissolving preweighed amounts of potassium dihydrogen phosphate (Riedel De Haen, KH_2PO_4, AnalaR grade) in double distilled water. Similarly, chloride stock and sulphate stock solutions were prepared by dissolving sodium chloride (NaCl) and sodium sulphate (Na_2SO_4), respectively in double distilled water.

2.1.3. Characterization of the water treatment sludge

Fourier transform infrared (FTIR) spectra of lime-iron sludge were examined using an FT-IR spectrometer (Thermo Scientific Nicolet iS5). The morphological structure of lime-iron sludge was examined using a scanning electron microscope (SEM; JEOL Scanning Electron Microscope JSM 6490 LV). The elemental composition of the sludge was determined using energy dispersive X-ray spectrometry (EDS).

2.2. Adsorption studies

2.2.1. Kinetic study

The effect of competing ions (Cl^- and SO_4^{2-}) was investigated at optimum operational conditions using an adsorbent mass of 0.5 g and synthetic phosphate solution (10.5 mg/L). The optimum operational conditions have been previously reported for phosphate adsorption onto lime-iron sludge [25] viz. pH 8.0; agitation 250 rpm; and equilibrium time of 16 h. After reaction, the adsorbent was separated by vacuum filtration using a Buchner's funnel and Whatman No. 3 qualitative filter paper. The concentration of phosphate in the filtrate was estimated by the Molybdate/Ascorbic Acid Method with Single Reagent (Method 365.2) using an ultraviolet spectrophotometer (Shimadzu Recording Spectrophotometer UV-1800). The amount of phosphate adsorbed per unit mass of adsorbent was obtained by:

$$q = \frac{(C_o - C_e)}{m} \times V \quad (1)$$

2.2.2. Equilibrium study

Batch equilibrium experiments were conducted by agitating reaction mixtures at 250 rpm for 16 h. The effect of initial phosphate concentration was studied by equilibrating adsorbent (5 g/L) in synthetic phosphate solution of varying concentrations (10 mg/L to 145.0 mg/L) at 298°K ± 2°K. The effect of adsorbent dose was studied by using varying adsorbent doses (3 g/L to 35 g/L) with synthetic phosphate solution (10.5 mg/L) at 298°K ± 2°K. The effect of temperature was studied by contacting the adsorbent with synthetic phosphate solution in a shaking water bath (Julabo SW23) at temperatures varying from 298°K ± 2°K to 328°K ± 2°K. The adsorption yield was calculated by:

$$\%\ \text{Adsorption} = \frac{(C_o - C_e)}{m} \times 100 \quad (2)$$

2.2.3. Desorption studies

After adsorption, the phosphate-saturated sludge was oven dried at 378 K for 24 h and then air dried (298°K ± 2°K) for 24 h. Desorption experiments were conducted using 0.25 g of saturated material spiked with an eluant (KCl, NaOH, and distilled water). Desorption efficiency was calculated by:

$$\text{Desorption\_Efficiency} = \frac{\text{Amount\_desorbed}}{\text{Amount\_adsorbed}} \times 100 \quad (3)$$

2.3. Kinetic models

2.3.1. Lagergren model

Lagergren's first-order rate equation describes the kinetic adsorption of oxalic acid and malonic acid onto charcoal [26]. The equation was later described as pseudo-first-order which can be represented as follows [27]:

$$q_t = q_e(1 - \exp^{-K_{PFO}t}) \quad (4)$$

2.3.2. Pseudo-second-order model

The pseudo-second-order equation was developed for the adsorption of divalent metal ions onto peat moss. The equation can be expressed as [28]:

$$q_t = \frac{K_{PSO}q_e^2 t}{1 + K_{PSO}q_e t} \quad (5)$$

$$h = (K_{PSO})q_e^2 \quad (6)$$

2.3.3. Intraparticle diffusion model

The model assumes that the rate of intraparticle diffusion varies proportionally with the half power of time. The model has the following form [29]:

$$q_t = K_{id}(t^{1/2}) \quad (7)$$

2.3.4. Diffusion-chemisorption model

The diffusion-chemisorption kinetic model was developed to simulate biosorption of heavy metals onto heterogeneous media. The model can be represented as follows [30]:

$$q_t = \frac{1}{\frac{1}{q_e} + \frac{t^{0.5-1}}{K_{DC}}} \quad (8)$$

$$k_i = K_{DC}^2 / q_e \quad (9)$$

2.4. Equilibrium models

2.4.1. Langmuir isotherm

The Langmuir isotherm assumes that adsorption sites on the adsorbent possess an equal affinity for molecules and that each site is capable of adsorbing one molecule thus forming a monolayer. The model is expressed as [31]:

$$q_e = \frac{q_m K_L C_e}{1 + K_L C_e} \quad (10)$$

The characteristic features of the Langmuir isotherm may be described in terms of the separation factor, R_L, a dimensionless constant given by Eq. (11) [32].

$$R_L = \frac{1}{(1 + K_L C_o)} \quad (11)$$

This separation factor can be used to describe further the nature of the adsorption process. The isotherm is unfavorable if $R_L > 1$; linear if $R_L = 1$; favorable if $0 < R_L < 1$ and irreversible if $R_L = 0$.

2.4.2. Freundlich isotherm

The Freundlich isotherm is an empirical model to describe adsorption onto heterogeneous surfaces as well as multilayer adsorption. The model is given by [33]:

$$q_e = K_F(C_e)^{1/n_F} \quad (12)$$

2.4.3. Redlich–Peterson isotherm

The Redlich–Peterson isotherm is a hybrid isotherm which incorporates the features of the Langmuir and the Freundlich isotherms. It is represented by [34]:

$$q_e = \frac{K_{RP}C_e}{1 + \alpha_{RP}C_e^{g_{RP}}} \quad (13)$$

2.4.4. Sips isotherm

The Sips isotherm is a combined form of the Langmuir and Freundlich isotherms developed for predicting heterogeneous adsorption systems and bypassing the limitation of the rising adsorbate concentration associated with Freundlich isotherm model [35]:

$$q_e = \frac{q_S(\alpha_S C_e)^{n_S}}{1 + (\alpha_S C_e)^{n_S}} \quad (14)$$

2.5. Thermodynamic equations

Thermodynamic parameters such as Gibbs free energy change $\Delta G°$, entropy change $\Delta S°$ and enthalpy change $\Delta H°$, describes the effect of temperature on the adsorption process. Where $\Delta G°$ is given by the following equation:

$$\Delta G° = -RT\ln K_L \quad (15)$$

According to Eq. (16) the slope and intercept obtained from linear plots of $\Delta G°$ versus temperature, T, represents $\Delta S°$ and $\Delta H°$, respectively.

$$\Delta G° = \Delta H° - T\Delta S° \quad (16)$$

Activation energy E_a and sticking probability S^* can be estimated using a modified Arrhenius-type equation related to surface coverage as:

$$S^* = (1-\theta)\exp(-E_a / RT) \tag{17}$$

which can be linearized as:

$$\ln(1-\theta) = \ln S^* + E_a / RT \tag{18}$$

where θ is the surface coverage as:

$$\theta = (1 - C_e / C_o) \tag{19}$$

According to Eq. (18), S^* and E_a can be determined from a plot of ln (1 – θ) versus 1/T. S^* can be used to gain further insight into the nature of the adsorption process. $S^* > 1$ describes adsorbate unsticking to adsorbent and thus no adsorption; $S^* = 1$ indicates a linear sticking relationship between adsorbate and adsorbent, possible mixture of physisorption and chemisorption; $S^* = 0$ suggests indefinite sticking of adsorbate to adsorbent, chemisorption mechanisms predominant; $0 < S^* < 1$ indicates favourable sticking of adsorbate to adsorbent, physisorption mechanism predominant [36].

2.6. Error analysis

The goodness of fit of the various kinetic, isotherm and ANN models to the experimental data were evaluated using the following expressions:

$$\chi^2 = \sum_{i=1}^{N} \frac{\left((q_{e_i})_{\text{predicted}} - (q_{e_i})_{\text{experimental}}\right)^2}{(q_{e_i})_{\text{predicted}}} \tag{20}$$

$$\text{RMSE} = \sqrt{\frac{1}{N}\sum_{i=1}^{N}\left((q_{e_i})_{\text{experimental}} - (q_{e_i})_{\text{predicted}}\right)^2} \tag{21}$$

$$\text{RPE \%} = \frac{\sum\left[\left|(q_e)_{\text{predicted}} - (q_e)_{\text{experimental}}\right| / (q_e)_{\text{experimental}}\right] * 100}{N} \tag{22}$$

$$\text{MSE} = \left(\frac{1}{N}\sum_{i=1}^{N}\left[t_i - y_i\right]^2\right) \tag{23}$$

$$R^2 = \frac{\sum_{i=1}^{N}\left(t_i - t_{\text{mean}}\right)^2 - \sum_{i=1}^{N}\left(y_i - y_i\right)^2}{\sum_{i-1}^{N}\left(t_i - y_i\right)^2} \tag{24}$$

2.7. ANN modeling

2.7.1. Development of an ANN model

ANNs are computational networks inspired by the functioning of the human nervous system. It utilizes previously solved examples to identify and learn input–output relationships and develop the ability to predict accurately new relationships.

In this study, the Neural Network Toolbox of MATLAB 7.14.0 (R2012a)® was used to develop a three-layer feed forward ANN model for predicting the phosphate adsorption capacity of lime-iron sludge. Initial phosphate concentration (10–182 mg/L), sludge dose (3–35 g) and temperature (298–328 K) were used as inputs to the network, and adsorption capacity was used as the output from the network. A total of 41 experimental sets obtained from batch equilibrium experiments were used to feed the network. The inputs and targets were first normalized in the range –1 to 1 to reduce the scaling effect of parameter values [37]. This was performed using the following equation:

$$X_{\text{norm}} = 2\left[\frac{X_i - X_{\min}}{X_{\max} - X_{\min}}\right] - 1 \tag{25}$$

where X_i is the input or output variable X, and $X_{\min}$ and $X_{\max}$ are the minimum and maximum value of variable X. The data set was subsequently divided into three sets: 70% of the data were applied to training the network, 15% for cross-validation and 15% for testing the accuracy of the neural network model and its prediction. Benchmark comparisons of learning algorithms followed by transfer functions (Eqs. (26)–(28)) were performed. Finally, optimization was carried out between the number of neurons in the hidden layer and the mean square error (MSE) for the best learning algorithm and transfer functions.

Logsig:

$$f(n) = 1/\left(1 + \exp(-n)\right) \tag{26}$$

Tansig:

$$f(n) = \left[2/\left(1 + \exp(-2 * n)\right)\right] - 1 \tag{27}$$

Purelin:

$$f(n) = n \tag{28}$$

2.7.2. Relative importance index

The relative importance of the input variables on the phosphate adsorption capacity was determined by sensitivity analysis using the neural network weight matrix and Garson's equation which can be expressed as follows:

$$Ij = \frac{\sum_{m=1}^{m=Nh}\left(\left(\left|W_{jm}^{ih}\right| \div \sum_{k=1}^{Ni}\left|W_{km}^{ih}\right|\right) \times \left|W_{mn}^{ho}\right|\right)}{\sum_{k=1}^{k=Ni}\left\{\sum_{m=1}^{m=Nh}\left(\left|W_{km}^{ih}\right| \div \sum_{k=1}^{Ni}\left|W_{km}^{ih}\right|\right) \times \left|W_{mn}^{ho}\right|\right\}} \tag{29}$$

where I_j is the relative importance of the j_{th} input variable on the output variable, N_i and N_h are the numbers of input and hidden neurons, respectively, W is the connection weight, the superscripts "i", "h" and "o" refer to input, hidden and

output layers, respectively, and subscripts "*k*", "*m*" and "*n*" refer to input, hidden and output neurons, respectively [38].

2.8. GA optimization

GA is a global optimization technique inspired by the evolutionary change of individual features as a result of reproduction and adaptation to new environment conditions and natural selection [15]. The algorithm starts with the random selection of a population of chromosomes known as the initial solution estimates, and the quality of this population is evaluated using a fitness function. The best-fitted chromosomes are selected for reproduction using different methods including stochastic uniform, remainder, uniform, shift linear, roulette and tournament. Random pairs of chromosomes are then chosen for mating whereby genes are exchanged with crossover to create new pairs of chromosomes [39]. This is performed using different methods including single point, double point or uniform crossover. The new chromosomes are then processed by the mutation operator whereby all or some of the genes of the parents are changed to increase the exploration of the genome such that the offsprings are not limited to the genes of the parents and may have new and better traits [40]. The quality of the offsprings is evaluated using the fitness function. The process is reiterated until an acceptable value of the fitness function is obtained [41]. In this study, the optimization toolbox of MATLAB 7.14.0 (R2012a)® was used to determine the optimum conditions for achieving maximum phosphate removal. The equation obtained from the ANN model was used as the fitness function and selection of GA parameters was done by trial and error.

3. Results and discussion

3.1. Performance comparison of lime-iron, lime and alum sludge

3.1.1. Equilibrium analysis using two and three-parameter models

The adsorption performance of lime-iron sludge was assessed through batch experiments and compared with that of alum and lime sludge both of which have been reported to successfully reduce phosphate concentration from solution. Analysis of the experimental data was carried out using the two-parameter Langmuir and Freundlich isotherms as well as the three-parameter Sips and Redlich–Peterson isotherms.

The applicability of these models to simulate the data was analyzed using non-linear regression. The goodness of fit of the models to the experimental data was assessed using the error functions presented as Eqs. (20)–(22). The results presented in Table 1 showed the Langmuir model was the best performing two-parameter models for all three sludges. A more robust simulation was observed by the three parameter models where the Redlich–Peterson isotherm provided the best correlation to the alum sludge. The Sips isotherm provided the best correlation to the lime sludge. This model produced the constant n_S to be 1.1087, indicating some degree of heterogeneity. Lime-iron sludge was best simulated using the Langmuir Isotherm. This implies that adsorption sites on the surface of the adsorbent may have equal affinity for phosphate and may be capable of adsorbing one phosphate anion, thus forming a monolayer.

The q_e values obtained in this study were compared with that of other adsorbents reported in the literature. The results presented in Table 1 indicate that lime-iron sludge produced the highest adsorption capacity of 15.3 mg/g. This was approximately 116% and 130% greater than that for lime sludge and alum sludge respectively. Table 2 reveals that lime-iron sludge exhibited an adsorption capacity for phosphate higher than several adsorbents reported in the literature; this further suggests its effectiveness as an adsorbent.

3.1.2. Adsorption affinity

The Langmuir isotherm produced a satisfactorily high correlation to all sludges, as such, K_L values are used in this section to compare and analyze adsorption affinity. Amongst the three sludges, lime-iron sludge exhibited the strongest affinity for the phosphate anion. Using the Langmuir constant K_L, the potential of the adsorbents for column application

Table 1
Comparison of isotherm models using non-linear regression to simulate uptake of phosphate

Adsorbent	Isotherm	Constants			X^2	RMSE	RPE
Alum sludge	Langmuir	q_m = 6.6519	K_L = 0.0349		0.0101	0.1438	3.7947
	Freundlich	K_F = 0.9229	n_F = 2.6537		0.0345	0.2919	7.9972
	Redlich	a_{RP} = 0.0035	K_{RP} = 0.1594	g_{RP} = 1.3936	0.0000	0.0543	1.2537
	Sips	α_S = 0.0465	q_S = 5.5931	n_S = 1.5299	0.0018	0.0661	1.2514
Lime sludge	Langmuir	q_m = 7.0863	K_L = 0.0833		0.0143	0.1019	1.5932
	Freundlich	K_F = 1.9420	n_F = 3.7902		0.1843	0.3212	5.9683
	Redlich	a_{RP} = 0.0499	K_{RP} = 0.4993	g_{RP} = 1.0727	1.4280	1.0282	16.6075
	Sips	α_S = 0.0874	q_S = 6.8649	n_S = 1.1087	0.0134	0.0945	1.5935
Lime-iron sludge	Langmuir	q_m = 15.2968	K_L = 0.1489		0.0626	0.2674	2.7056
	Freundlich	K_F = 4.3808	n_F = 3.4820		1.1776	0.9255	10.4658
	Redlich	a_{RP} = 0.1730	K_{RP} = 2.4113	g_{RP} = 0.9780	0.1424	0.4396	3.8479
	Sips	α_S = 0.1453	q_S = 15.4631	n_S = 0.9709	0.0669	0.2652	2.8981

was further assessed by calculating the dimensionless constant separation factor R_L (Eq. (11)). Within the range of initial phosphate concentration investigated the values of R_L for alum varied from 0.5624 to 0.1857, lime sludge from 0.3477 to 0.0799 and lime-iron sludge from 0.2424 to 0.0448. This implied that all sludges produce favorable isotherms and are appropriate phosphate adsorbents. However, lime-iron sludge produced the lowest R_L which suggests that it is the most favourable adsorbent for column applications.

Table 2
Comparison of the phosphate adsorption capacity by various adsorbents reported in the literature

Adsorbent	q_e (mg/g)	Reference
Goethite	6.420	[42]
Natural zeolite	2.150	[43]
Na-natural zeolite	2.190	[44]
Iron oxide tailings	8.210	[45]
SCS (synthetic iron oxide coated sand)	1.500	[46]
CB (coated crushed brick)	1.750	[46]
NCS (naturally iron oxide coated sand)	0.880	[46]
Alum sludge	6.6519	This study
Lime sludge	7.0863	This study
Lime-iron sludge	15.2968	This study

3.1.3. Characteristics of lime-iron sludge

SEM images illustrated in Figs. 1(a) and (b) were used to examine the surface morphology of lime-iron sludge. Before adsorption, a rough surface was observed, and sludge particles appeared amorphous, with irregular flocs. The SEM image after adsorption seems less amorphous and smooth in some areas. The change in surface morphology was more accurately assessed by calculating the fractal dimension, D_f, of the SEM images using the Box Counting method. Fractal analysis is a non-traditional mathematical procedure which measures complexity as a fractal dimension. A high fractal dimension is indicative of a rough surface. In this study, the Box-Counting method in Matlab 7.14.0 (R2012a)® was used to determine the fractal dimension of lime-iron sludge before and after adsorption. The SEM images were first converted to

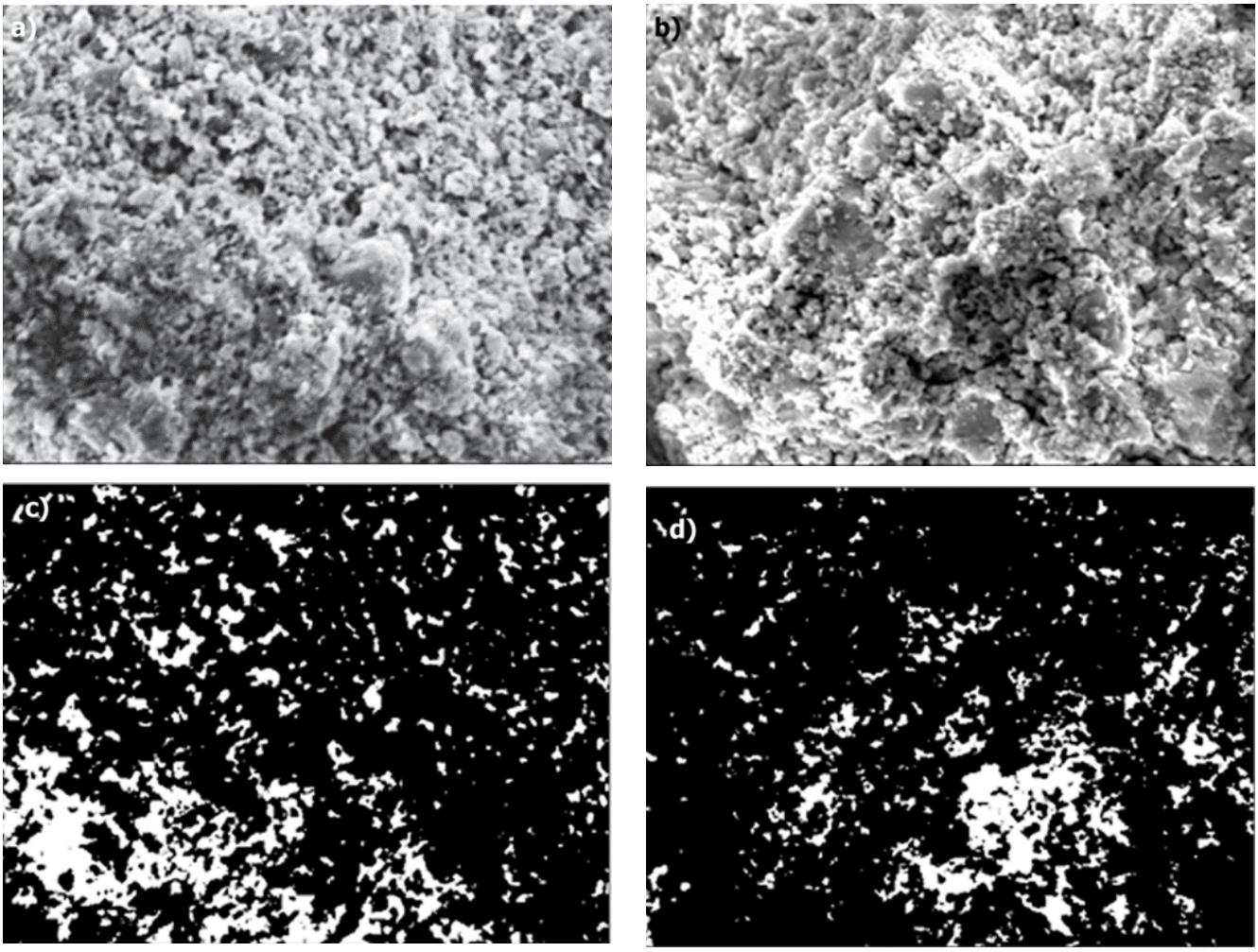

Fig. 1. (a) SEM of powdered lime-iron sludge before adsorption, (b) SEM of powdered lime-iron sludge after adsorption, (c) binary image of lime-iron sludge before adsorption and (d) binary image of lime-iron sludge after adsorption.

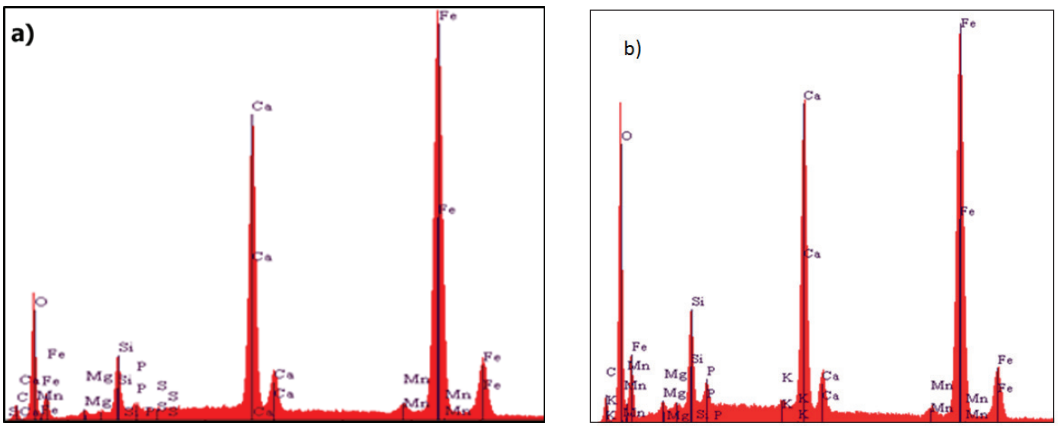

Fig. 2. EDS spectrum of powdered lime-iron sludge (a) before adsorption and (b) after adsorption.

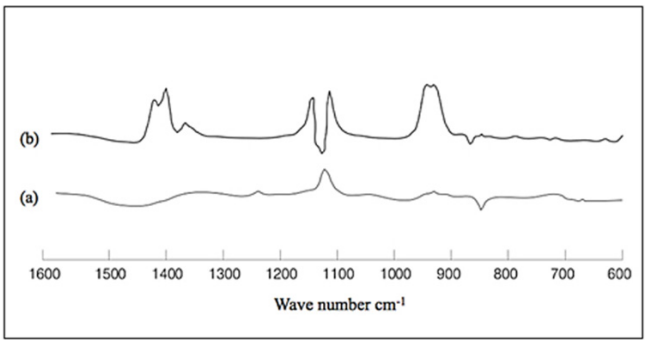

Fig. 3. FTIR spectra of lime-iron sludge (a) before adsorption and (b) after adsorption.

binary images and the number of boxes needed to completely cover the fractal was determined. The process was repeated with different box sizes. A plot of box size (x-axis) against the number of boxes needed to cover the fractal (y-axis) was carried out to obtain a logarithmic function. The slope of this function is referred to as the box dimension which is taken as an approximation of the fractal dimension. The binary images before and after adsorption are shown in Figs. 1(c) and (d), respectively. Prior to adsorption, D_f was 1.7133 and reduced to 1.6403 after adsorption. This decrease in fractal dimension indicates smoothing of the surface which may have resulted from the saturation of available binding sites on the surface of the material. The energy dispersive spectrum (EDS) shown in Figs. 2(a) and (b) was used to determine the elemental composition of the sludge. The spectrum reveals that Fe, Ca, S and O were the dominant elements present before and after adsorption. The high presence of oxygen shown often presumes their occurrence in the oxide and oxo-hydroxide form. Additionally, the EDS exposes the presence of small concentrations of phosphate prior to adsorption. The increase in intensity of the phosphate peak after adsorption confirms that phosphate was successfully adsorbed onto the sludge.

The Fourier transform infrared (FTIR) spectra of lime-iron sludge before and after adsorption were taken to identify the presence of functional groups involved in the process (Fig. 3). The spectra revealed the development of strong bands within 850 and 1,250 cm^{-1} after adsorption. This range of frequencies corresponds to phosphate stretching [47]. The different band positions in this range may be attributed to the species of phosphate present as well as the mineral composition of the adsorbent. $H_2PO_4^-$ occurs at a frequency of 1,127 cm^{-1} [48]. At the reaction mixture pH of 7.4, $H_2PO_4^-$ is the dominant specie and hence accounts for the intense band after adsorption. The small bands at 1,135 cm^{-1} prior to adsorption indicates the presence of a small concentration of phosphate in lime-iron sludge. Another characteristic feature in the spectra is the appearance of bands in the region 1,250–1,600 cm^{-1} specifically at 1,350 and 1,420 cm^{-1}. These bands may be attributed to C–O stretching.

3.2. Development of a predictive model for lime-iron sludge

3.2.1. Selection of backpropagation algorithm

The effect of sludge dose, initial adsorbate concentration and adsorbent dose on adsorption capacity was studied at the optimum agitation; pH and contact time reported and used to develop a three-layer feed-forward ANN to predict the adsorption capacity of lime-iron sludge. The performance of 11 backpropagation algorithms was first evaluated to determine the best algorithm for training the network (Table 3). Using the tansig and purelin transfer functions at the hidden and output layer respectively and 10 neurons at the hidden layer, the Levenberg–Marquardt algorithm produced the lowest MSE of 0.1404 and highest R^2 of 0.9995.

3.2.2. Selection of transfer function

The impact of three commonly used transfer functions [Eqs. (26)–(28)] was then assessed. Using the Levenberg–Marquardt algorithm and 10 neurons in the hidden layer, the best performance was obtained using the tansig transfer function at the hidden layer and the purelin transfer function at the output layer (Table 4).

3.2.3. Optimization of the number of neurons in the hidden layer

Finally, the number of hidden neurons was varied from 2 to 17 and its influence on performance assessed using the MSE. The network was trained using Levenberg-Marquardt algorithm with the tansig and purelin transfer functions at

Table 3
Comparison of various backpropagation algorithms

Backpropagation (BP) algorithms	Function	MSE	R^2
BFGS quasi-Newton backpropagation	Trainbfg	0.3448	0.9919
Powell–Beale conjugate gradient backpropagation	Traincgb	0.6306	0.9895
Fletcher–Reeves conjugate gradient backpropagation	Traincgf	0.5995	0.9900
Polak–Ribiere conjugate gradient BP	Traincgp	0.8085	0.9897
Gradient descent	Traingd	155.6050	0.6099
Gradient descent with momentum	Traingdm	155.6050	0.6099
Gradient descent with momentum and adaptive learning	Traingdx	6.0465	0.8572
Levenberg–Marquardt backpropagation	Trainlm	0.1404	0.9995
One step secant backpropagation	Trainoss	0.6835	0.9886
Resilient backpropagation	Trainrp	3.6839	0.9557
Scaled conjugate gradient backpropagation	Trainsgc	0.5199	0.9883

Table 4
Relationship between transfer function and training of the network with respect to MSE

Hidden layer transfer function	Output layer transfer function	MSE
Logsig	Logsig	28.3853
Logsig	Purelin	1.5025
Logsig	Tansig	0.1514
Purelin	Logsig	24.4395
Purelin	Purelin	3.2763
Purelin	Tansig	0.7269
Tansig	Logsig	4.5006
Tansig	Purelin	0.1404
Tansig	Tansig	0.1637

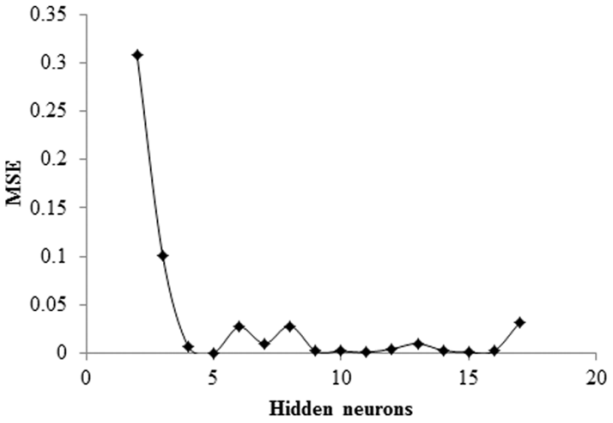

Fig. 4. Effect of the number of neurons in the hidden layer on the performance of the ANN.

the hidden and output layer respectively. The results presented in Fig. 4 reveals the expected decrease in MSE with increasing number of neurons. The fluctuations in MSE between 5 and 9 neurons and an increase beyond 16 neurons may have resulted from the network being trapped into the local minima [49]. The minimum MSE value of 0.001 was obtained using 11 hidden neurons and was selected as the optimum number for the network.

Fig. 5 shows the optimized ANN architecture of the network. Using this optimized ANN, the predicted q_e was compared with the experimental q_e using the coefficient of determination which produced an R^2 value of 0.9994. The optimized ANN model was also compared with the Langmuir isotherm. As shown in Figs. 6(a)–(d) for all temperatures studied the ANN model provided a more accurate simulation of the experimental data.

3.2.4. Empirical equation

An empirical equation correlating the input parameters was developed to predict adsorption capacity without having to run the ANN model in Matlab. The equation derived using the weights (W_i) and biases (b_i) to the input layer of the optimized network (Table 5) is presented here as follows:

$$\begin{aligned} q_{t\,pred} = &-0.45503F_1 + 0.074313F_2 + 0.13809F_3 - 0.02419F_4 \\ &+ 0.056989F_5 + 0.10945F_6 - 1.1947F_7 - 0.18769F_8 \\ &+ 0.32535F_9 + 0.051549F_{10} - 0.18586F_{11} - 1.0231 \end{aligned} \quad (30)$$

where coefficients are the weights and bias to the output layer and F_i is the *tansig* activation function used in the hidden layer and is given as:

$$F_i = \frac{2}{\left[1+\exp(-2*E_i)\right]} - 1;\ i = 1:11 \quad (31)$$

and E_i is the weighted sum of the input defined as:

$$E_i = W_{i1} \times C_o + W_{i2} \times M + W_{i3} \times T + b_i \quad (32)$$

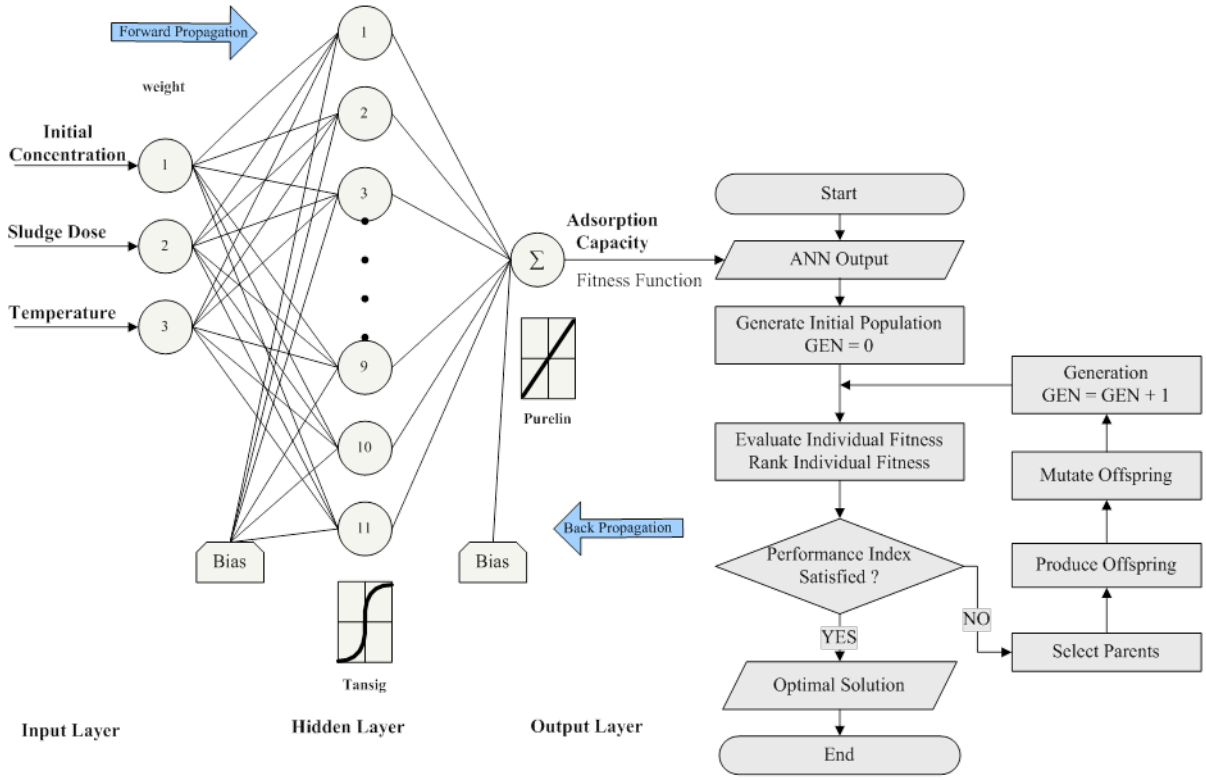

Fig. 5. Optimized ANN and GA architecture.

3.2.5. Relative importance index

The relative importance of the input variables on the output was determined using the Garson's equation. The results indicated that initial phosphate concentration had a relative importance of 44.79% and thus was the most influential parameter in the adsorption process. Sludge dose and temperature exhibited a relative importance of 30.14% and 25.07%, respectively. This underscores the significance of concentration gradient which impacts the driving force for adsorption.

3.2.6. Process optimization using GA

GA methodology was used to determine the optimum initial phosphate concentration, sludge dose, and temperature necessary to achieve maximum phosphate removal. The ANN model (Eq. (30)) was used as the fitness function which determines how close a given combination of operational parameters are towards achieving maximum adsorption. It can be defined as follows:

$$\text{Fitness function} = \text{purelin}\left(LW * \text{tansig}\left(IW * [x(1); x(2); x(3)] + b1\right) + b2\right) \quad (33)$$

where IW and b1 are the weight and bias of the hidden layer and LW and b2 are the weight and bias of output layers presented in Table 5.

Optimization was performed using a double vector population type with a generation and population size of 100. Crossover fraction and mutation rate were set as default, i.e., 0.8 and 0.2, respectively. The selection, crossover and mutation operators selected by a trial and error process were stochastic uniform, scattered and constraint dependent, respectively. Fig. 7 presents the fitness values versus generation. After approximately 15 generations, the value of fitness reached to a minimum value and then remained constant.The developed ANN-GA predicted a maximum removal of 18.36 mg/g using an initial phosphate concentration of 59 mg/L, sludge dose of 3 g and temperature of 325 K. Subsequent laboratory experimentation to validate the model prediction was performed at these optimal operational conditions. The resulting experimental adsorption was 18.12 mg/g, generating a residual error of 1.3%. This reveals a good agreement with the ANN-GA optimized results and thus confirms the validity of the ANN-GA model.

3.3. Equilibrium experiments and analysis

3.3.1. Effect of initial phosphate concentration on adsorption

The effect of initial phosphate concentration as a function of both the percentage adsorbed at equilibrium and the amount adsorbed per unit mass of adsorbent is presented in Fig. 8. The figure reveals a decrease in removal from 91% to 48% as adsorbate concentration was increased from 10.5 mg/L to 144.0 mg/L. The significant reduction in percentage adsorption may be attributed to the insufficient number of adsorption sites to accommodate the large number of phosphate anions present at higher concentrations. The results, therefore, suggest that this adsorbent is well suited to treat water bodies with low phosphate concentration including domestic wastewater which usually contains 4–15 mg/ L total phosphate [50].

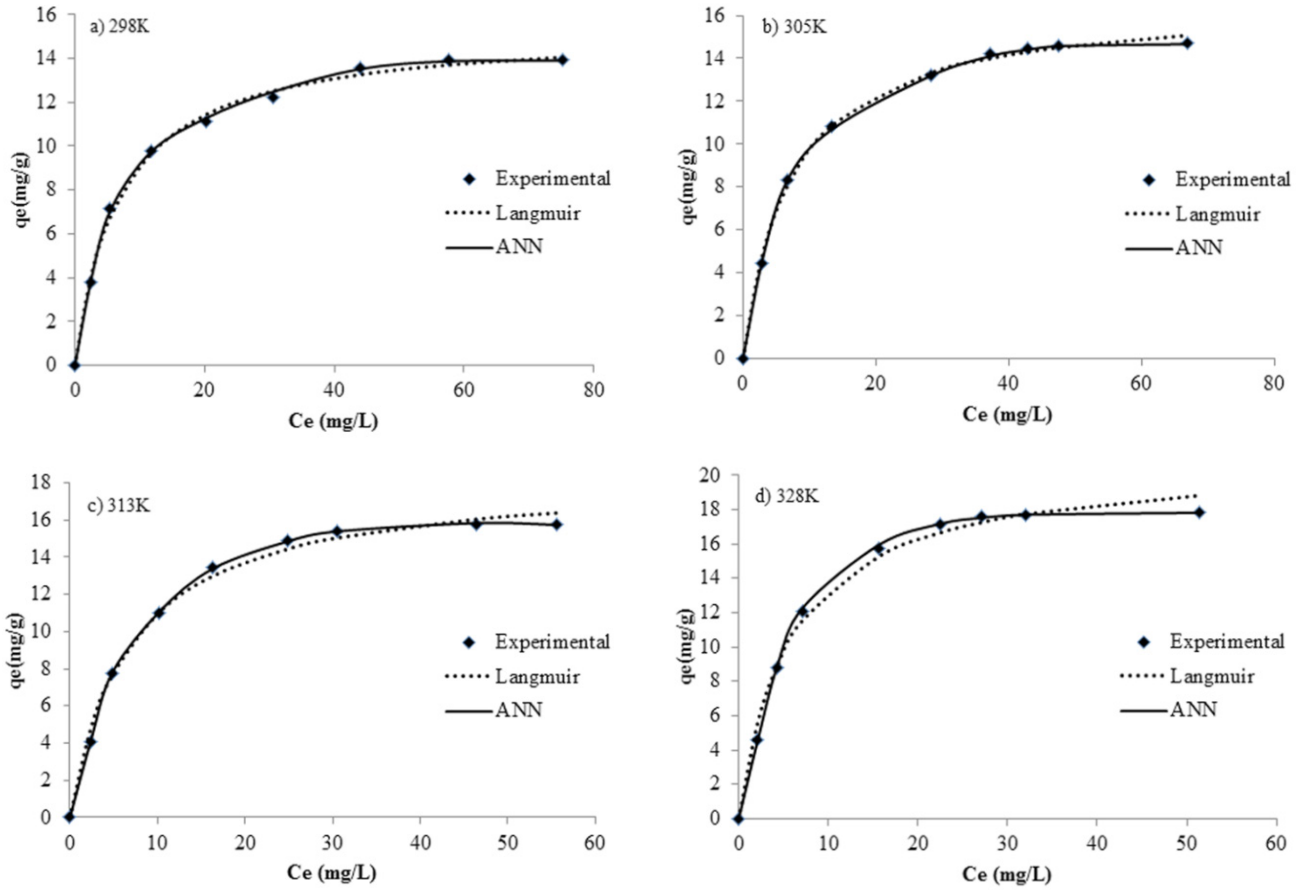

Fig. 6. Plots showing goodness of fit of ANN and Langmuir model to experimental data at (a) 298 K, (b) 305 K, (c) 313 K and (d) 328 K.

Table 5
Weight and bias values obtained by the Levenberg–Marquardt algorithm with 11 neurons

I	W_{i1}	W_{i2}	W_{i3}	B_i
1	1.5390	2.1524	1.6770	–3.1341
2	1.3384	2.0120	1.7255	–2.6038
3	–2.4873	0.0653	–0.3065	1.6439
4	1.0185	2.2961	1.5822	–1.7123
5	–1.5540	–4.0907	4.1926	–2.5456
6	–3.2382	–0.9772	–0.1084	0.4056
7	–1.0099	0.5838	0.3450	–0.3383
8	–1.5800	0.1622	–3.7184	2.7665
9	1.2445	1.5052	0.9441	1.6636
10	1.1214	0.8291	–2.0355	2.5319
11	–3.0935	–2.1396	–1.2453	–5.1948

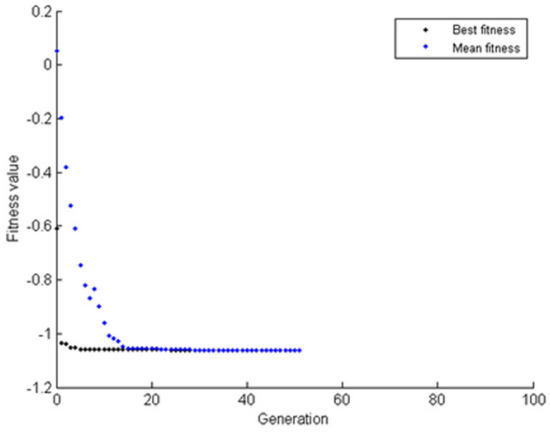

Fig. 7. Fitness values versus generation.

The increase in phosphate concentration from 10.5 mg/L to 111 mg/L resulted in a sharp increase in the uptake of phosphate per mass of lime-iron sludge. Higher initial adsorbate concentration creates a steeper concentration gradient which provides a greater driving force to overcome mass transfer resistance of adsorbate ions from the liquid to the solid phase [51]. This consequently increases the diffusion of adsorbate ions to adsorption sites and thus results in an increase in the unit mass saturation of the adsorbent. Minimum increase in adsorption capacity beyond 111 mg/L may be attributed to saturation of most of the adsorptions sites.

3.3.2. Effect of adsorbent dose on adsorption

The effect of adsorbent dose as a function of both the percentage of phosphate adsorbed at equilibrium and the mass of phosphate adsorbed per gram of lime-iron sludge is presented in Fig. 9. An increase in sludge dose from 3 g/L to 10 g/L resulted in 12% increase in adsorption capacity. This increase may be attributed to the availability of a greater number of adsorption sites with increasing sludge dose. The increase in sludge dose beyond 10 g/L resulted in marginal increases in adsorption. This behavior may be due to the binding of almost all phosphate anions to the sludge and the establishment of equilibrium.

As the sludge dose increases, the amount of phosphate adsorbed per gram of sludge decreases. At low sludge dose, the adsorption capacity is high due to the saturation of the finite number of adsorption sites available. Increasing in sludge dose, increases the number of available adsorption sites. Thus, the probability of saturation of all adsorption sites per gram of adsorbent decreases. This decrease was most significant as sludge dose increased from 3 g/L to 15 g/L.

3.3.3. Effect of temperature on adsorption

The effect of temperature was investigated at an initial phosphate concentration (10.5 mg/L) and sludge dose (5 g/L). Increase in temperature from 298 K to 328 K resulted in 20% increase in adsorption capacity (Table 6) which suggests that the adsorption process was endothermic. This favorable effect of temperature can increase the kinetic energy of the adsorbate ions which in turn increases its collision onto adsorption sites.

To further expound the effect of temperature, the Gibbs free energy change $\Delta G°$, enthalpy change $\Delta H°$ and entropy change $\Delta S°$ were calculated using Eqs. (15) and (16). The results are presented in Table 6. Within the range of temperature studied $\Delta G°$ varied between –20 kJ/mol and 0 kJ/mol and $\Delta H°$ was less than 4.2 kJ/mol. This implies that adsorption was spontaneous and occurred via physical forces [52]. Additionally, the positive value of $\Delta H°$ suggests that the process is endothermic with the presence of an energy barrier. The positive $\Delta S°$ reflects the high affinity of lime-iron sludge for phosphate anions.

The predominance of physical adsorption was further assessed by calculating the activation energy E_a and the sticking probability S^* using the modified Arrhenius-type equation. Low E_a values (5–40 kJ/mol) denotes physisorption and is indicative of a diffusion controlled process [36]. Further, it suggests that the energy barrier existing between the reactants is relatively low. The E_a value was found to be 9.6634 kJ/mol while the sticking probability was found to be 0.0104. This implies that the likelihood of phosphate anions attaching to the lime-iron sludge is high and further confirms that physisorption is the predominant attachment mechanism.

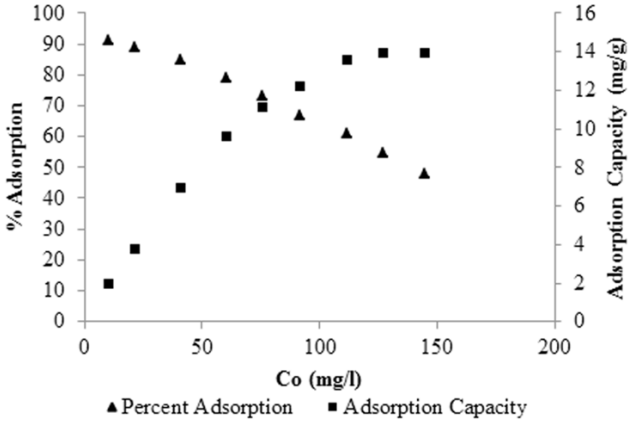

Fig. 8. Effect of initial phosphate concentration on the uptake by lime-iron sludge.

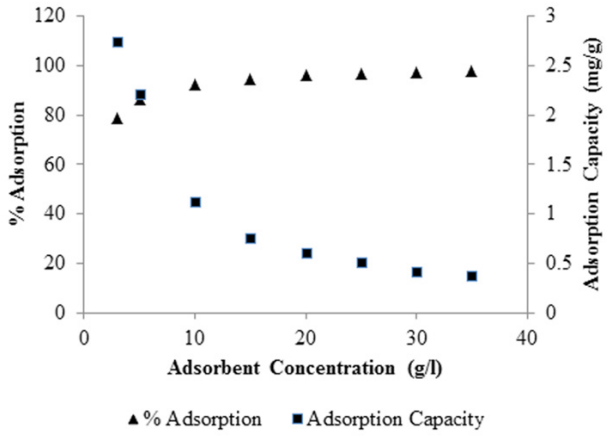

Fig. 9. Effect of adsorbent dose on the uptake of phosphate by lime-iron sludge.

Table 6
Thermodynamic parameters for phosphate adsorbed on water treatment sludge

Temperature (K)	q_m (mg/g)	K_a (L/mol)	$\Delta G°$ (kJ/mol)	ΔS (kJ/mol)	ΔH (kJ/mol)	E_a (kJ mol^{-1})	S^*
298	15.3490	13.7517	–6.4941	5.3428	0.0393	9.6634	0.0104
305	16.7024	13.1913	–6.5412				
313	18.3675	14.0176	–6.8708				
328	20.9507	16.3348	–7.6173				

3.4. Kinetics experiments and analysis

3.4.1. Effect of competing ions on adsorption

The kinetic effect of competing ions was investigated using a constant initial phosphate concentration of 10.5 mg/L and equal concentrations of chloride and sulphate ions. Experimental data were fitted to the pseudo-first-order model, pseudo-second-order model, intraparticle diffusion model and the diffusion-chemisorption model. Non-linear regression analysis revealed that the pseudo-second-order model provided the best correlation for samples without competing anions (R^2 = 0.9994) while the diffusion-chemisorption model produced the best correlation in the presence of competing ions (R^2 = 0.9972–0.9980).

The diffusion-chemisorption model also produced a high correlation in the absence of competing ions and was therefore used to assess the overall impact of competing ions. As shown in Table 7, the presence of varying concentrations of equal parts chloride and sulphate resulted in only marginal fluctuations in the relative sorption capacity. There was no consistent trend in initial rate, k_i, and overall rate, K_{DC}, observed over the range of competing ions. At a stock solution pH 7.3–8.4, a fraction of the phosphate occurs as the monovalent specie $H_2PO_4^-$ and the remaining fraction as the divalent HPO_4^{2-}. Therefore, chloride being monovalent may have a lower affinity for iron oxide present in the sludge than divalent sulphate and phosphate. Even though a fraction of the phosphate exists as the monovalent specie, it interacts more strongly with iron than sulphate. Thus, the presence of such competing ions had a negligible effect on the process [53].

3.4.2. Desorption experiments and analysis

Desorption studies were conducted using three common eluants namely, NaOH, KCl, and distilled water. Approximately 99% of phosphate was desorbed by 0.2 M NaOH within the first 10 min of reaction. Distilled water removed 40% of phosphate after 1 h while 0.3 M KCl released approximately 40% phosphate after 50 min. The partial phosphate desorption by KCl and distilled water may be due to the presence of less tightly bound phosphate ions on the adsorbent (non-specific adsorption). At low surface loading, phosphate preferentially occupies the high-affinity adsorption sites with a high binding energy. This is mainly in the form of specific adsorption or inner-sphere complexation, resulting in a minimal percentage desorption. With increased phosphate loading, the nonspecific adsorption (outer-sphere complexation) of phosphate increases [54].

The effectiveness of NaOH in desorbing phosphate may be attributed to the high pH, where OH^- ions, the dominant anion species, compete with $H_2PO_4^-$ for active sites on the sludge surface. Therefore, the results suggest that phosphate adsorption onto lime-iron sludge may be reversible and may involve both inner-sphere and outer-sphere complexation.

3.5. Mechanism of adsorption

Transfer of ions from a liquid phase to a solid phase usually involves a transportation stage followed by an attachment stage. Thermodynamics analysis revealed that physisorption (due to relatively weak van der Waals forces) was the dominant attachment mechanism. Desorption studies indicated that this process may be reversible and may involve both inner-sphere and outer-sphere complexation. Kinetic data were analyzed according to the intraparticle diffusion model by Weber and Morris to determine the dominant transportation mechanism. The plot of q_t vs. $t^{1/2}$ (Fig. 10) reveals distinct linear stages suggesting that three steps occurred during the adsorption process. The first linear phase which occurs within the first hour of reaction may be attributed to film diffusion or surface adsorption while the second linear phase may be attributed to intraparticle diffusion. The third slope may be ascribed to the slowing of adsorption rate possibly due to a reduction in the concentration gradient.

4. Conclusion

The adsorption behavior of lime-iron sludge was investigated as a reuse option for sludge generated at a plant in central Trinidad. The sludge exhibited a phosphate adsorption capacity of 15.3 mg/g which compares well with other reported adsorbents in the literature. Additionally, the sludge revealed a high affinity for the phosphate anion whereby competing ions had an insignificant effect on adsorption. The adsorbed phosphate was effectively desorbed (99%) using 0.2 M NaOH. The attachment mechanism of phosphate onto lime-iron sludge was attributed to physical forces while the transport of phosphate to the adsorption site was influenced by both film and intraparticle diffusion.

Table 7
Kinetic parameters of adsorption obtained by non-linear regression

Cl^- and SO_4^{2-} ions (mg/L)	Initial rate, k_i, (mg/g-t)	Overall rate, K_{DC}, (mg/g-t)	Relative adsorption capacity, q_e, (mg/g)
0	9.9939	4.7424	2.2504
300	14.2414	5.4417	2.0793
400	13.6069	5.3232	2.0825
500	13.4695	5.296	2.0823
750	7.9717	4.1332	2.1430
1,000	9.2823	4.4200	2.1047

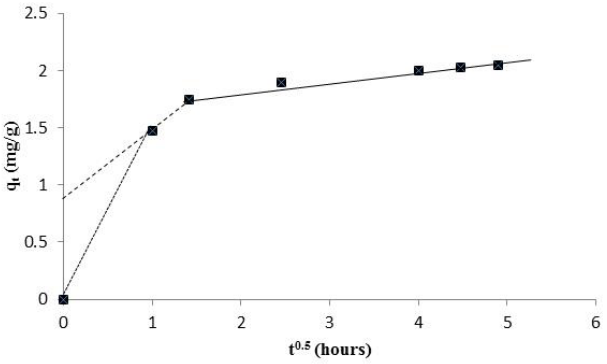

Fig. 10. Plot of intraparticle diffusion model.

The Langmuir isotherm model provided the highest correlation to the equilibrium data while the diffusion-chemisorption model provided the highest correlation to the kinetic data. A predictive model for phosphate adsorption capacity was successfully developed using ANN and optimized using GA. The accuracy of the ANN-GA prediction was verified by experimental studies which revealed a residual error of 1.3%.

Symbols

C_o	—	initial concentration, mg/L
C_e	—	final concentration, mg/L
V	—	volume, L
M	—	mass, g
K_{PFO}	—	pseudo-first-order rate constant, min^{-1}
q_t	—	adsorption capacity at time t, mg/g
q_e	—	equilibrium adsorption capacity, mg/g
t	—	reaction time, hours
K_{PSO}	—	pseudo-second-order rate constant, g/mg-min
H	—	pseudo-second-order initial adsorption rate, mg/g-t
K_{id}	—	intraparticle transport rate constant, mg/g-$t^{1/2}$
K_{DC}	—	diffusion-chemisorption constant, mg/g-$t^{0.5}$
k_i	—	diffusion-chemisorption initial adsorption rate, mg/g-t
B	—	rate coefficient related to the effective diffusion coefficient
F	—	fractional attainment of equilibrium
K_L	—	Langmuir adsorption equilibrium constant, L/mg
K_F	—	Freundlich constant related to adsorption affinity, mg/g
n_F	—	Freundlich constant related to heterogeneity
K_{RP}	—	Redlich–Peterson equilibrium constant
g_{RP}	—	Redlich–Peterson exponent
α_{RP}	—	Redlich–Peterson constant
a_s	—	Sips affinity constant
n_s	—	Sips index of heterogeneity
R	—	universal gas constant, 8.314 J/Kmol
T	—	absolute temperature, K

References

[1] D. Cordell, T.S.S. Neset, Phosphorus vulnerability: a qualitative framework for assessing the vulnerability of national and regional food systems to the multidimensional stressors of phosphorus scarcity, Glob. Environ. Chang., 24 (2014) 108–122.

[2] M.R. Awual, A. Jyo, Assessing of phosphorus removal by polymeric anion exchangers, Desalination, 281 (2011) 111–117.

[3] L.E. De-Bashan, Y. Bashan, Fertilizer Potential of Phosphorus Recovered from Wastewater Treatments, First International Meeting of Microbial Phosphate Solubilisation, 2007, pp. 179–184.

[4] M.W. Kamiyango, S.M.I. Sajidu, W.R.L. Masamba, Removal of phosphate ions from aqueous solutions using bauxite obtained from Mulanje, Malawi, Afr. J. Biotechnol., 10 (2011) 11972–11982.

[5] W.T. Mohammed, S.A. Rashid, Phosphorus removal from wastewater using oven-dried alum sludge, Int. J. Chem. Eng., 2012 (2012) 1–11.

[6] P. Tang, Utilisation of Sargassum Polycystum for Removal of Malachite Green and Methylene Blue, B. Eng Thesis, Kuala Lumpur, University Tunku Abdul Rahman, 2011.

[7] L. Johansson, J.P. Gustafsson, Phosphate removal using blast furnace slags and Opoka-mechanism, Wat. Res., 34 (2000) 259–265.

[8] L. Zheng, L. Xiaomei, J. Liu, Adsorptive removal of phosphate from aqueous solutions using iron oxide tailings, Wat. Res., 38 (2004) 1381–1326.

[9] J. Chen, H. Kong, D. Wu, X. Chen, D. Zhang, Z. Sun, Phosphate immobilization from aqueous solution by fly ashes in relation to their composition, J. Hazard. Mater. B, 139 (2007) 293–300.

[10] J. Pradhan, J. Das, S. Das, R.S. Thakur, Adsorption of phosphate from aqueous solution using activated red mud, J. Colloid Interface Sci., 204 (1998) 169–172.

[11] J.G. Kim, J.H. Kim, H.S. Moon, C.M. Chon, J.S. Ahn, Removal capacity of water plant alum sludge for phosphorus in aqueous solutions, Chem. Spec. Bioavailab., 14 (2003) 67–73.

[12] D. Schimmel, K.C. Fagnani, J.B. Oliveira dos Santos, M.A.S.D. Barros, E. Antonio da Silva, Adsorption of Turquoise Blue QG on Commercial Activated Carbon in Batch Reactor: Kinetic and Equilibrium Studies, Braz. J. Chem. Eng., 27 (2010) 289–298.

[13] T.A.H. Nguyen, H.H. Ngo, W.S. Guo, T.Q. Pham, F.M. Li, T.V. Nguyen, X.T. Bui, Adsorption of phosphate from aqueous solutions and sewage using zirconium loaded okara (ZLO): fixed-bed column study, Sci. Total Environ., 523 (2015) 40–49.

[14] S.N.A. Abas, M.H.S. Ismail, M.L. Kamal, S. Izhar, Adsorption process of heavy metals by low-cost adsorbent: a review, World Appl. Sci. J., 28 (2013) 1518–1530.

[15] A.M. Ghaedi, M. Ghaedi, A.R. Pouranfard, A. Ansari, Z. Avazzadeh, A. Vafaei, I. Tyagi, S. Agarwal, V.K. Gupta, Adsorption of triamterene on multi-walled and single-walled carbon nanotubes: artificial neural network modeling and genetic algorithm optimization, J. Mol. Liq., 216 (2016) 654–665.

[16] K. Yetilmezsoy, S. Demirel, Artificial neural network (ANN) approach for modeling of Pb(II) adsorption from aqueous solution by Antep pistachio (*Pistacia vera* L.) shells, J. Hazard. Mater., 153 (2008) 1288–1300.

[17] M.R. Fagundes-Klen, P. Ferri, T.D. Martins, C.R.G. Tavares, E.A. Silva, Equilibrium study of the binary mixture of cadmium-zinc ions biosorption by the *Sargassum filipendula* species using adsorption isotherms models and neural network, Biochem. Eng. J., 34 (2007) 136–146.

[18] V.K. Pareek, M.P. Brungs, A.A. Adesina, R. Sharma, Artificial neural network modeling of a multiphase photodegradation system, J. Photochem. Photobiol. A Chem., 149 (2002) 139–46.

[19] P. Koehn, Combining Genetic Algorithms and Neural Networks: The Encoding Problem, MSc. Thesis, Knoxville, The University of Tennessee, 1994.

[20] X. Deng, Y. Ye, Proc. Internet and Network Economics: First International Workshop, WINE 2005, Hong Kong, China, 2005.

[21] Y. Yasin, F.B.H. Ahmad, M. Ghaffari-Moghaddam, M. Khajeh, Application of a hybrid artificial neural network–genetic algorithm approach to optimize the lead ions removal from aqueous solutions using intercalated tartrate-Mg–Al layered double hydroxides, Environ. Nanotechnol. Monit. Manage., 1–2 (2014) 2–7.

[22] M. Ghaedi, N. Zeinali, A.M. Ghaedi, M. Teimuori, J. Tashkhourian, Artificial neural network-genetic algorithm based optimization for the adsorption of methylene blue and brilliant green from aqueous solution by graphite oxide nanoparticle, Spectrochim. Acta Mol. Biomol. Spectrosc., 125 (2014) 264–277.

[23] M. Molashahi, H. Hashemipour, Experimental study and artificial neural network simulation of methane adsorption on activated carbon, Korean J. Chem. Eng., 29 (2012) 601–605.

[24] D. Benny, Engineering Appraisal of Iron and Manganese Removal Plants in Trinidad, MPhil Thesis, Trinidad, University of the West Indies, 2007.

[25] B.S. Chittoo, C. Sutherland, Adsorption of phosphorus using water treatment sludge, J. Appl. Sci., 24 (2014) 3455–3463.

[26] S. Lagergren, About the theory of so-called adsorption of soluble substances, K. Sven. Vetensk. Akad. Handl., 24 (1898) 1–39.

[27] Y.S. Ho, G. McKay, Sorption of dye from aqueous solution by peat, Chem. Eng. J., 70 (1998) 115–124.

[28] Y.S. Ho, G. McKay, Kinetic model for lead (II) sorption onto Peat, Adsorpt. Sci. Technol., 16 (1998) 243–255.
[29] W.J. Weber, C.J. Morris, Advances in Water Pollution Research: Removal of Biologically Resistant Pollutants from Waste Waters by Adsorption, Proc. Int. Conf. on Water Pollution Symposium, Pergamon Press, Oxford, 2, 1962, pp. 231–266.
[30] C. Sutherland, C. Venkobachar, A diffusion-chemisorption kinetic model for simulating biosorption using forest macro-fungus *Fomes fasciatus*, Int. J. Plant Sci., 1 (2010) 107–117.
[31] I. Langmuir, The adsorption of gases on plane surface of glass, mica and platinum, J. Am. Chem. Soc., 40 (1916) 1361–1368.
[32] K. Hall, L.C. Eagleton, A. Acrivos, T. Vermeulen, Pore- and solid-diffusion kinetics in fixed bed adsorption under constant-pattern conditions, Ind. Eng. Chem. Fund., 5 (1966) 212–223.
[33] H.M.F. Freundlich, Over the adsorption in solution, J. Phys. Chem., 57 (1906) 385–470.
[34] O. Redlich, D.L. Peterson, A useful adsorption isotherm, J. Phys. Chem., 63 (1959) 1024–1026.
[35] R. Sips, Combined form of Langmuir and Freundlich Eqs., J. Chem. Phys., 16 (1948) 490–495.
[36] H. Nollet, M. Rols, P. Lutgen, P. Van der Meeren, W. Verstraete, Removal of PCBs from wastewater using fly ash, Chemosphere., 52 (2003) 655–665.
[37] S. Chowdhury, S. Chakraborty, S.D. Papita, Removal of crystal violet from aqueous solution by adsorption onto eggshells: equilibrium, kinetics, thermodynamics and artificial neural network modeling, Waste Biomass Valor., 4 (2013) 655–664.
[38] G. Garson, Interpreting neural-network connection weights, Artif Intell Expert., 6 (1991) 46–51.
[39] L.I. Moralesa, R.A. Conde-Gutiérreza, J.A. Hernándezb, A. Huicocheab, D. Juárez-Romerob, J. Siqueirosc, Optimization of an absorption heat transformer with two-duplex components using inverse neural network and solved by genetic algorithm, Appl. Therm. Eng., 85 (2015) 322–333.
[40] M. Bagheri, S.A. Mirbagheri, Z. Bagheri, A.M. Kamarkhani, Modeling and optimization of activated sludge bulking for a real wastewater treatment plant using hybrid artificial neural networks-genetic algorithm approach, Process Saf. Environ., 95 (2015) 12–25.
[41] E.T. Tomczak, W.L. Kaminski, Application of genetic algorithms to determine heavy metal ions sorption dynamics on clinoptilolite bed, Chem. Process Eng., 33 (2012) 103–116.
[42] O.K. Borggaard, B. Raben-Lange, A.L. Gimsing, B.W. Strobel, Influence of humic substances on phosphate adsorption by aluminium and iron oxides, Geoderma., 127 (2005) 270–279.
[43] K. Sakadevan, H.J. Bavor, Phosphate adsorption characteristics of soils, slags and zeolite to be used as substrates in constructed wetland systems, Water Res., 32 (1998) 393–399.
[44] D. Wu, B. Zhang, C. Li, Z. Zhang, H. Kong, H. Simultaneous removal of ammonium and phosphate by zeolite synthesized from fly ash as influenced by salt treatment, Colloid Int. Sci., 304 (2006) 300–306.
[45] L. Zeng, X. Li, J. Liu, Adsorptive removal of phosphate from aqueous solutions using iron oxide tailings, Water Res., 38 (2004) 1318–1326.
[46] N. Boujelben, J. Bouzid, E. Elouear, M. Feki, F. Jamoussi, A. Montiel, Phosphate removal from aqueous solution using iron coated natural and engineered sorbents, J. Hazard. Mater., 151 (2008) 103–110.
[47] T.T. Zheng, Z.X. Sun, X.F. Yang, A. Holmgren, Sorption of phosphate onto mesoporous γ-alumina studied with in-situ ATR-FTIR spectroscopy, Chem. Cent. J., 6 (2012) 26–36.
[48] P.R. Rout, P. Bhunia, R.R. Dash, Modeling isotherms, kinetics and understanding the mechanism of phosphate adsorption onto a solid waste: ground burnt patties, J. Env. Chem. Eng., 2 (2014) 1331–1342.
[49] Z. Shahryari, A. Sharifi, A. Mohebbi, Artificial neural network (ANN) approach for modeling and formulation of phenol adsorption onto activated carbon, J. Eng. Thermophys. Rus., 22 (2013) 322–336.
[50] G. Akay, B. Keskinler, A. Cakici, U. Danis, Phosphate removal from water by red mud using crossflow microfiltration, Water Res., 32 (1998) 717–726.
[51] N. Tewari, P. Vasudevan, B.K. Guha, Study on biosorption of Cr (VI) by Mucor Hiemalis, Biochem. Eng. J., 23 (2005) 185–192.
[52] D. Suteu, T. Malutan, Industrial cellolignin waste as adsorbent for methylene blue dye from aqueous solutions, Bio Resources., 8 (2013) 427–446.
[53] L.T. Lee, P. Somasundaran, Effects of inorganic and organic additives on the adsorption of nonionic polyacrylamide on hematite, J. Colloid Interface Sci., 142 (1991) 470–479.
[54] X. Wang, F. Liu, W. Tan, W. Li, X. Feng, D.L. Sparks, Characteristics of phosphate adsorption-desorption onto ferrihydrite: comparison with well-crystalline Fe (hydr) oxides, Soil Sci., 178 (2013) 1–11.